analytical chemistry

pubs.acs.org/ac Article

DNA Three-Way Junction with Multiple Recognition Regions Mediated an Unconfined DNA Walker for Electrochemical Ultrasensitive Detection of miRNA-182-5p

Yuanyuan Chang, Sai Xu, Yunrui Li, Wenxi Hu, Hang Li, Ruo Yuan,* and Yaqin Chai*

Cite This: *Anal. Chem.* 2021, 93, 12981−12986 Read Online

ACCESS | Metrics & More | Article Recommendations | Supporting Information

ABSTRACT: In this work, a DNA three-way junction (TWJ) with multiple recognition regions was intelligently engineered, which could be applied as an unconfined DNA walker with a rapid walking speed and high sensitivity for electrochemical detection of microRNA (miRNA-182-5p). Once the target miRNA was presented, the hairpins on TWJ could be successively opened to form an annular DNA walker, which could walk on the entire scope of the electrode surface without the confine for the length of DNA walker legs compared with the traditional DNA walker, greatly improving the walking efficiency. In addition, this DNA walker with multirecognition segments could obviously increase the local concentration of recognition sites, which significantly enhanced the detection speed and sensitivity. As a result, this proposed biosensor with annular DNA as a walker could dexterously achieve the ultrasensitive and fast detection of miRNA-182-5p from 0.1 fM to 1 nM with a detection limit of 31.13 aM. Meaningfully, this strategy explored an innovative path in the design of a new DNA walker nanostructure for accomplishing speedy and sensitive detection of biomarkers.

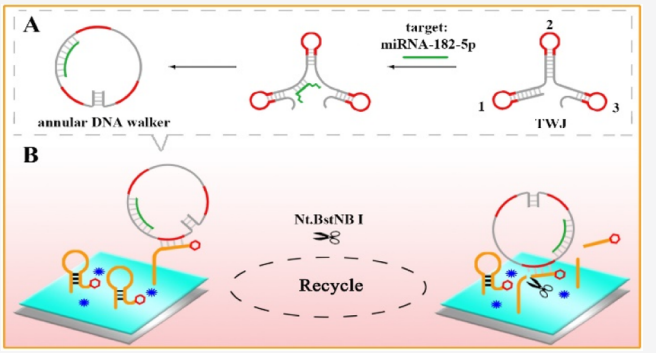

INTRODUCTION

Over the past several decades, DNA was employed as a superior biocompatible building material for the construction of diverse dynamic nanodevices containing DNA robots,[1,2] DNA tweezers,[3,4] and DNA walkers[5−8] due to its excellent physicochemical stability, sequence programmability, and accurate Watson−Crick base pairing.[9−11] Thereinto, the intelligent DNA walker had gained attractive attention and was extensively applied in molecular sensing,[12−14] bioimaging,[15,16] and drug delivery,[17] which was generally powered by nicking endonucleases, DNAzymes, or strand displacement to manipulate specific DNA (walking leg) for autonomously moving. Although the traditional DNA walker that walked along a one-dimensional track or a two-dimensional surface improved the detection sensitivity and efficiency up to a point,[18−20] there still remained two critical challenges: first, the walking legs with a limited length made the DNA walker inclined to derail from the track and stall in a region of the locally depleted substrate, resulting in the unsatisfactory walking efficiency.[21−23] Second, since the single DNA walker with only a single recognition site dramatically hindered the effective collision between targets and DNA walking legs, the promotion of the corresponding detection speed and sensitivity was limited vastly. Thus, it is of urgent necessity to innovate a special DNA walker which could achieve the unconfined walking with multiple recognition regions to overcome these problems.

Herein, an annular DNA walker with three recognition zones mediated by the DNA three-way junction (TWJ) was intelligently exploited for rapid and sensitive electrochemical detection of miRNA-182-5p, which is closely related to several cancers.[24,25] The detection principle is displayed in Scheme 1. First, the DNA single strand was annealed into a TWJ with the recognition regions locked in hairpin stems. Once the target miRNA-182-5p was introduced, the hairpins could be opened stepwise, further triggering the formation of an annular DNA walker with the exposure of three recognition sequences. Subsequently, the DNA walker would open the hairpin H modified with ferrocence (Fc) on the depAu/GCE surface to generate duplex DNAs that could be cleaved by Nt.BstNB I endonuclease, simultaneously releasing the DNA walker to participate in the next recycle and the Fc-labeled DNA fragment away from the electrode surface. Consequently, after the electrochemical signal was obviously decreased, the

Received: June 24, 2021
Published: September 13, 2021

https://doi.org/10.1021/acs.analchem.1c02668
Anal. Chem. 2021, 93, 12981−12986

Scheme 1. Schematic Illustration of the As-Prepared Electrochemical Biosensor for the Detection of miRNA-182-5p: (A) Assembly of the TWJ-Mediated Annular DNA Walker and (B) Construction of the Electrochemical Biosensor and Signal Response

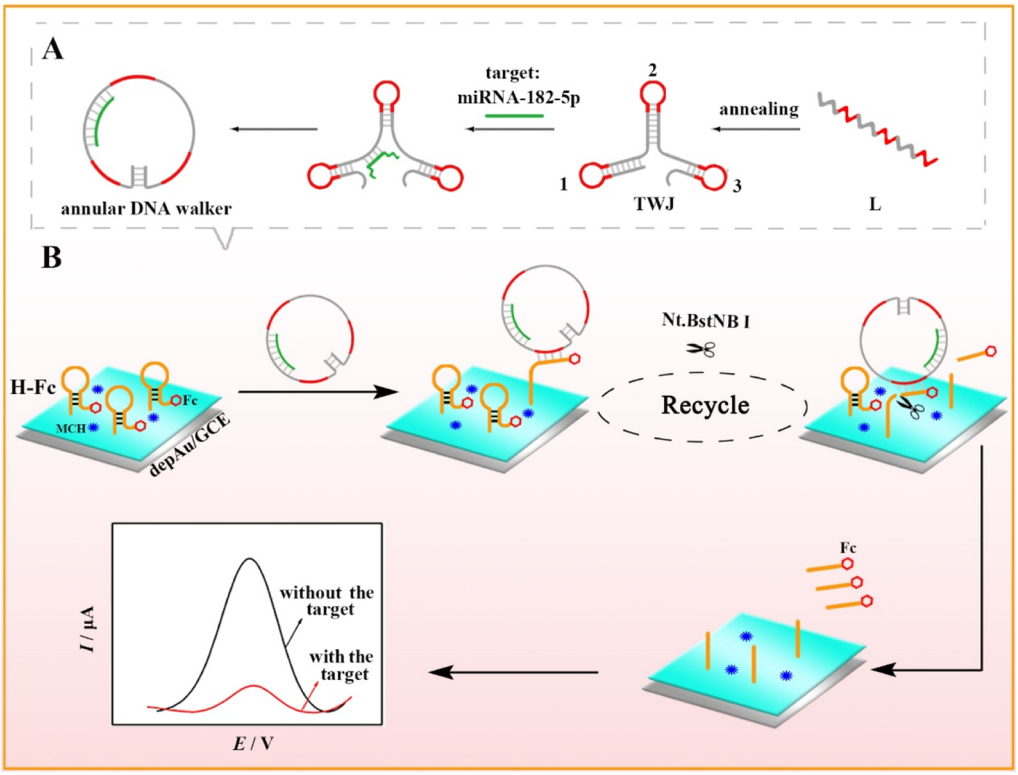

ultrasensitive detection for target miRNA could be achieved. This way, the novel unconfined annular DNA walker with multirecognition regions could avoid the restriction of the walking-leg length, rapidly accomplishing the continuous walking on the entire area of the electrode surface and significantly increasing the detection speed and sensitivity. Above all, this strategy provided a unique avenue to innovatively design a nanostructure for the unconfined DNA walker in ultrasensitive and speedy detection of biomarkers and possessed great potential in clinical diagnosis of diseases.

EXPERIMENTAL SECTION

Assembly of the DNA TWJ and Hairpin H-Fc. In short, 10 μL of DNA strand L (2 μM) and H-Fc (2 μM) were respectively heated to 95 °C for 10 min and subsequently cooled for 1 h to obtain the stable stem-loop TWJ and hairpin H-Fc. Afterward, target miRNA-182-5p was added to open three hairpins on TWJ (2 μM) to form the annular DNA walker. The reagents and apparatus used in this work are displayed in the Supporting Information, and the oligonucleotide sequences applied in this work are presented in Table S1.

Fabrication of the Proposed Biosensor. First, the cleaned electrode by 0.3 and 0.05 μm alumina slurry was electrodeposited with a layer of gold nanoparticles (depAu) for 30 s in $HAuCl_4$ (1%) solution at −0.2 V. Straight after, the obtained hairpin H-Fc (10 μL) was interacted onto depAu/GCE overnight, which could generate an obvious electrochemical signal. Next, MCH (10 μL) was dropped onto the electrode surface (H-Fc/depAu/GCE) for 20 min to block the nonspecifically adsorbed DNAs. Subsequently, 20 μL of the above-obtained mixture of TWJ and target miRNA-182-5p was added onto the electrode (MCH/H-Fc/depAu/GCE) to open the annealed hairpin H-Fc for 2 h (37 °C). At last, the modified electrode (TWJ/MCH/H-Fc/depAu/GCE) was incubated with the Nt.BstNB I enzyme (5 μL, 8 U μL^{-1}) at 55 °C to cleave one H-Fc DNA strand at its recognition sequence (5′-GAGTC-3′),[26,27] resulting in the release of the DNA fragment labeled with Fc. Then, the annular DNA walker could react with the other H-Fc DNA strand, in which the H-Fc DNA was cleaved with the help of the Nt.BstNB I enzyme for the next cycling. Finally, a decreased electrochemical signal could be gained. The optimization of the experimental conditions is shown in Figure S1.

RESULTS AND DISCUSSION

Polyacrylamide-Gel Electrophoresis (PAGE). Polyacrylamide-gel electrophoresis (PAGE) was adopted to characterize the successful construction of the annular DNA walker. As shown in Figure 1, the results show that the band in lane 1 represented the target miRNA-182-5p, which was ascribed to the low molecular weight. Meanwhile, the bright band in lane 2 corresponded to TWJ. Subsequently, after the target miRNA-182-5p was hybridized with TWJ at 37 °C for 2 h, the highest band with the slowest migration could be noticed (lane 3), suggesting that the annular DNA walker could be successfully assembled with the help of target miRNA-182-5p.

Electrochemical Characterization of the Proposed Biosensor. When depAu was immobilized on the electrode surface by electrodeposition, the electrochemical signal of $[Fe(CN)_6]^{3-/4-}$ significantly increased (Figure 2A, curve b) compared with the bare GCE (Figure 2A, curve a) because of the good conductivity of depAu. Subsequently, the electrochemical signal dramatically decreased (curve c) after the H DNA strand was successfully fixed on the electrode owing to

https://doi.org/10.1021/acs.analchem.1c02668
Anal. Chem. 2021, 93, 12981−12986

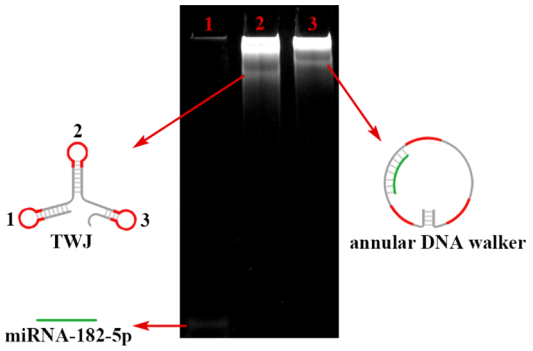

Figure 1. PAGE results for different samples: lane 1, target miRNA-182-5p (2 μM); lane 2, TWJ (2 μM); and lane 3, target miRNA-182-5p (2 μM) and TWJ (2 μM).

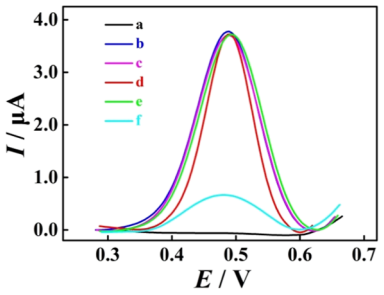

Figure 3. SWV responses of different sensing electrodes: (a) depAu/GCE, (b) MCH/H-Fc/depAu/GCE, (c) target + TWJ/MCH/H-Fc/depAu/GCE, (d) target + Nt.BstNB I/MCH/H-Fc/depAu/GCE, (e) TWJ + Nt.BstNB I/MCH/H-Fc/depAu/GCE, and (f) TWJ + Nt.BstNB I + target/MCH/H-Fc/depAu/GCE.

the fact that the electron transfer could be hindered by the DNA phosphate backbone with a negative charge. Subsequently, the introduction of MCH could lead to an obvious reduction in electrochemical signal (curve d) because the assembly of MCH could offer a stratum compactum, efficiently resisting the nonspecific adsorption of the noncomplementary or complementary sequences.[28] Finally, the electrochemical signal also showed a successive decrease when TWJ was dropped onto the electrode (curve e).

Furthermore, electrochemical impedance spectroscopy (EIS) was employed to prove the successful construction of this as-prepared biosensor. As shown in Figure 2B, a small semicircle domain and a long tail were displayed with the bare GCE (curve a). Then, an obviously reduced semicircle diameter was revealed (curve b) after depAu was introduced onto the electrode surface due to the excellent conductivity of depAu. After that, the successive enhanced R_{et} could be obtained when H, and MCH and TWJ were gradually dropped onto the electrode surface (curve *c*–*e*), attributing to the increasing block from DNAs and MCH. The results of EIS were kept up with that of cyclic voltammetry (CV), further proving that the as-prepared biosensor was successfully constructed. Furthermore, we have performed scanning electronic microscopy and atomic force microscopy to demonstrate the successful assembly of dep-Au on the GCE surface (see Figure S2).

Feasibility of the As-Prepared Biosensor for MiRNA-182-5p Detection. To demonstrate the feasibility of the developed biosensor based on the annular DNA walker for detecting the target miRNA-182-5p, square-wave voltammetry (SWV) measurements were carried out in PBS solution for different modified electrodes. As displayed in Figure 3, no SWV signal was detected with depAu/GCE (curve a) due to the absence of electroactive materials. However, an obvious electrochemical signal (Fc, 0.49 V) was recorded (curve b) after the Fc-labeled H (H-Fc) was immobilized onto the electrode surface, which suggested that H-Fc was successfully self-assembled on depAu/GCE to generate an initial current response. Subsequently, the SWV response of the electrode (curve c) did not show obvious change after the TWJ (2 μM) and target miRNA-182-5p (100 pM) were incubated on the electrode surface in the absence of the Nt.BstNB I enzyme, illustrating that the Fc-labeled DNA could not be released from the electrode surface without the nicking enzyme. Once the biosensor was immobilized with target miRNA-182-5p (100 pM) and the Nt.BstNB I enzyme (8 U μL^{-1}) without TWJ, the SWV response (curve d) remained almost unchanged compared with the initial signal (curve b). Similarly, the SWV response (curve e) nearly kept the same with the initial one (curve b) in the presence of TWJ (2 μM) and the Nt.BstNB I enzyme (8 U μL^{-1}) but without target miRNA-182-5p. Surprisingly, once the target miRNA-182-5p (100 pM), TWJ (2 μM), and Nt.BstNB I (8 U μL^{-1}) were simultaneously presented, the SWV response significantly decreased (curve f), which illustrated that the proposed biosensor was able to be successfully applied for ultrasensitive miRNA-182-5p detection.

Analytical Performance of the Proposed Biosensor. Different concentrations of miRNA-182-5p were measured to value the analytical performance of this as-prepared biosensor under optimal experiment conditions. As shown in Figure 4A, the SWV responses significantly decreased with the addition of gradually increased concentrations of miRNA-182-5p, showing strong correlation between electrochemical responses and the logarithm (*lg*) of miRNA-182-5p concentration in the range of 0.1 fM to 1 nM (Figure 4B). Also, the regression equation

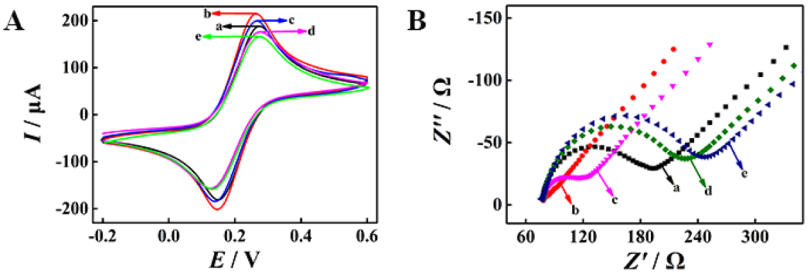

Figure 2. (A) CV and (B) EIS responses of (a) bare GCE, (b) depAu/GCE, (c) H/depAu/GCE, (d) MCH/H/depAu/GCE, and (e) TWJ/MCH/H/depAu/GCE.

https://doi.org/10.1021/acs.analchem.1c02668
Anal. Chem. 2021, 93, 12981−12986

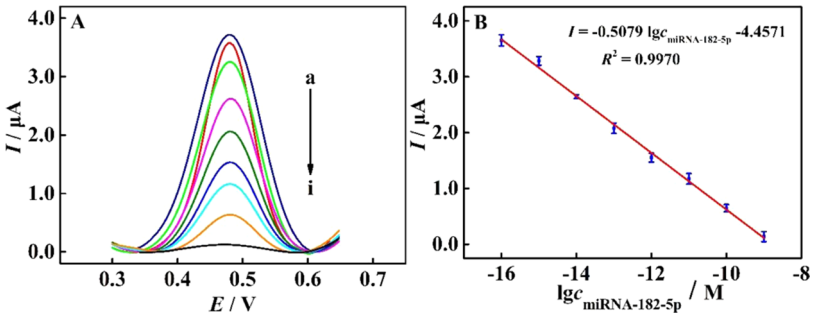

Figure 4. (A) SWV responses of the as-prepared biosensor for miRNA-182-5p detection at (a) 0 fM, (b) 0.1 fM, (c) 1 fM, (d) 10 fM, (e) 100 fM, (f) 1 pM, (g) 10 pM, (h) 100 pM, and (i) 1 nM. (B) Corresponding calibration plots of I vs lg $c_{miRNA\text{-}182\text{-}5p}$. Error bars, SD, n = 3.

could be expressed as $I = -0.5079 \lg c_{miRNA\text{-}182\text{-}5p} - 4.4571$ with a correlation-coefficient value (R^2) of 0.9970 and a detection limit of 31.13 aM (LOD = $3S_b/m$, with m representing the slope of the fitted curve and S_b representing the standard deviation of the blank signals).[29,30] Moreover, the as-prepared biosensor for miRNA-182-5p detection was compared with other conventional biosensors, and showed better analytical performance for biomarkers detection (Table 1), attributing to the enhanced local concentrations and the high walking speed of this annular DNA walker.

Table 1. Comparison of Other Methods for Biomarker Detection

target	analytical method	liner range	detection limits	reference
miRNA-21	FL	2−40 pM	2.14 fM	31
miRNA-141	FL	1 pM−2.5 nM	0.21 pM	32
miRNA-21	DPV	5 fm−100 pM	2.2 fM	33
ctDNA	DPV	1 fM−10 nM	0.29 fM	34
miRNA-21	SWV	0.5 fM−100 nM	0.25 fM	35
miRNA-196b	SWV	1.0 pM−10 nM	0.26 pM	36
miRNA182-5p	SWV	0.1 fM−1 nM	31.13 aM	this work

Selectivity, Stability, and Applications of the Proposed Biosensor. For investigating the selectivity of the proposed electrochemical biosensor, miRNA-155 (100 pM), miRNA-21 (100 pM), and miRNA-203a (100 pM) were chosen as interfering molecules. As exhibited in Figure 5A, even with the concentrations of interfering molecules (miRNAs) as high as 100 pM, the electrochemical signal changes of miRNA-21, miRNA-155, and miRNA-203a were negligible compared to the blank. However, the current response value rapidly decreased once a little amount of miRNA-182-5p (1 pM) was mixed with these interfering molecules (miRNAs), implying that this as-prepared electrochemical biosensor possessed a high selectivity toward miRNA-182-5p detection. Furthermore, we also stored this proposed biosensor at 4 °C and monitored every 5 days to evaluate the stability of the biosensor. After the storage for about 20 days, the signal responses were still kept at 96.61−103.34% of the initial one (Figure 5B), which suggested the excellent stability of this biosensor. In addition, to estimate the application of the as-prepared biosensor for miRNA-182-5p detection in real samples, we performed recovery experiments through adding a series of miRNA-182-5p with different concentrations of 10 fM, 1 pM, and 10 pM into human serum and detected using this developed biosensor. The calculated relative standard deviations (RSDs) and the rate of recoveries were satisfying ranging from 3.5 to 5.2% and from 93.4 to 106.0%, as listed in Table 2, respectively, indicating the capable applicability and reliability of this electrochemical biosensor for miRNA-182-5p monitoring in real samples.

Table 2. Recovery Tests of miRNA-182-5p in Human Serum with the Proposed Biosensor

sample	added	found (average)	RSD (%)	rate of recovery (%)
1	10 fM	9.64 fM	3.5	93.4−106.0
2	1 pM	0.993 pM	3.6	94.6−103.1
3	100 pM	99.3 pM	5.2	93.6−101.1

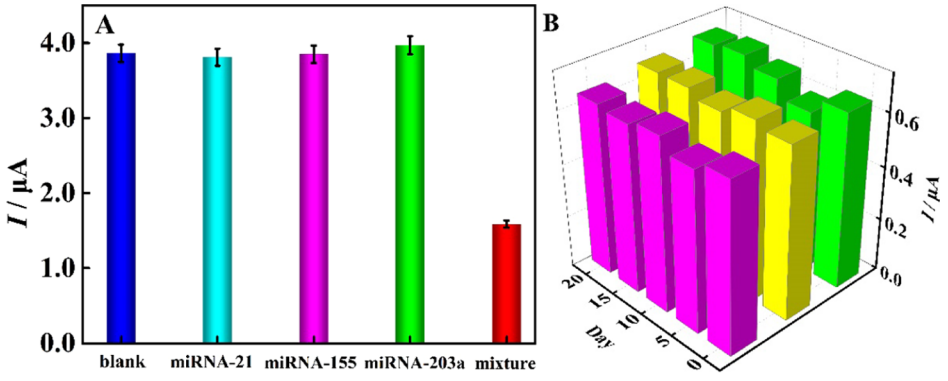

Figure 5. (A) Specificity of the biosensor when employed with targets of miRNA182-5p against other interfering miRNAs of miRNA-21, miRNA-155, and miRNA-203a. (B) Stability of the as-prepared electrochemical biosensor.

https://doi.org/10.1021/acs.analchem.1c02668
Anal. Chem. 2021, 93, 12981−12986

CONCLUSIONS

In summary, an eye-catching electrochemical biosensor was successfully established for ultrasensitive and rapid detection of miRNA-182-5p with the help of a DNA TWJ which could trigger the formation of an annular DNA walker. Surprisingly, this proposed strategy reflected two laudable merits as follows: first, the annular DNA walker could achieve the constant walking on the entire scope of the electrode surface without the limitation of DNA walker legs compared with traditional DNA walkers, greatly improving the walking efficiency and decreasing the detection limit. Second, the innovative employment of the TWJ with multiple recognition regions dramatically increased the local concentrations of recognition sequences, which accelerated the reaction speed and improved the detection efficiency. Above all, this proposed strategy put forward a new horizon in the design of a multifunctional DNA walking machine for the DNA self-assembly amplification technology in the detection of biomarkers.

ASSOCIATED CONTENT

Supporting Information

The Supporting Information is available free of charge at https://pubs.acs.org/doi/10.1021/acs.analchem.1c02668.

Reagents, apparatus, optimization of the experimental conditions, and characterization of depAu (PDF)

AUTHOR INFORMATION

Corresponding Authors

Ruo Yuan − *Key Laboratory of Luminescence Analysis and Molecular Sensing (Southwest University), Ministry of Education, College of Chemistry and Chemical Engineering, Southwest University, Chongqing 400715, PR China;* orcid.org/0000-0003-3664-6236; Phone: +86 2368252277; Email: yuanruo@swu.edu.cn; Fax: +86 2368253172

Yaqin Chai − *Key Laboratory of Luminescence Analysis and Molecular Sensing (Southwest University), Ministry of Education, College of Chemistry and Chemical Engineering, Southwest University, Chongqing 400715, PR China;* orcid.org/0000-0003-4392-9592; Phone: +86 2368252277; Email: yqchai@swu.edu.cn; Fax: +86 2368253172

Authors

Yuanyuan Chang − *Key Laboratory of Luminescence Analysis and Molecular Sensing (Southwest University), Ministry of Education, College of Chemistry and Chemical Engineering, Southwest University, Chongqing 400715, PR China*

Sai Xu − *Key Laboratory of Luminescence Analysis and Molecular Sensing (Southwest University), Ministry of Education, College of Chemistry and Chemical Engineering, Southwest University, Chongqing 400715, PR China*

Yunrui Li − *Key Laboratory of Luminescence Analysis and Molecular Sensing (Southwest University), Ministry of Education, College of Chemistry and Chemical Engineering, Southwest University, Chongqing 400715, PR China*

Wenxi Hu − *Key Laboratory of Luminescence Analysis and Molecular Sensing (Southwest University), Ministry of Education, College of Chemistry and Chemical Engineering, Southwest University, Chongqing 400715, PR China*

Hang Li − *Key Laboratory of Luminescence Analysis and Molecular Sensing (Southwest University), Ministry of Education, College of Chemistry and Chemical Engineering, Southwest University, Chongqing 400715, PR China;* orcid.org/0000-0002-8486-6631

Complete contact information is available at: https://pubs.acs.org/10.1021/acs.analchem.1c02668

Notes

The authors declare no competing financial interest.

ACKNOWLEDGMENTS

This paper was financially supported by the National Natural Science Foundation of China (21974108 and 21775124), the China Postdoctoral Science Foundation (2019M663417 and 2020T130544), and the Postdoctoral Science Foundation of Chongqing Natural Science Foundation (cstc2020jcyj-bsh0026), China.

REFERENCES

(1) Tang, J.; Yao, C.; Gu, Z.; Jung, S.; Luo, D.; Yang, D. *Angew. Chem., Int. Ed.* **2020**, *59*, 2490−2495.

(2) Ma, W.; Zhan, Y.; Zhang, Y.; Shao, X.; Xie, X.; Mao, C.; Cui, W.; Li, Q.; Shi, J.; Li, J.; Fan, C.; Lin, Y. *Nano Lett.* **2019**, *19*, 4505−4517.

(3) Zhang, P.; Jiang, J.; Yuan, R.; Zhuo, Y.; Chai, Y. *J. Am. Chem. Soc.* **2018**, *140*, 9361−9364.

(4) Liu, M.; Jiang, S.; Loza, O.; Fahmi, N. E.; Šulc, P.; Stephanopoulos, N. *Angew. Chem.* **2018**, *130*, 9485−9489.

(5) Jiang, J.; Zhang, P.; Nie, Y.-m.; Peng, K.-f.; Zhuo, Y.; Chai, Y.-q.; Yuan, R. *Chem. Sci.* **2020**, *11*, 2193−2199.

(6) Qu, X.; Zhu, D.; Yao, G.; Su, S.; Chao, J.; Liu, H.; Zuo, X.; Wang, L.; Shi, J.; Wang, L.; Huang, W.; Pei, H.; Fan, C. *Angew. Chem., Int. Ed.* **2017**, *56*, 1855−1858.

(7) Yao, D.; Bhadra, S.; Xiong, E.; Liang, H.; Ellington, A. D.; Jung, C. *ACS Nano* **2020**, *14*, 4007−4013.

(8) Zhao, L.; Sun, R.; He, P.; Zhang, X. *Anal. Chem.* **2019**, *91*, 14773−14779.

(9) Feldkamp, U.; Niemeyer, C. M. *Angew. Chem., Int. Ed.* **2006**, *45*, 1856−1876.

(10) Kwon, P. S.; Ren, S.; Kwon, S.-J.; Kizer, M. E.; Kuo, L.; Xie, M.; Zhu, D.; Zhou, F.; Zhang, F.; Kim, D.; Fraser, K.; Kramer, L. D.; Seeman, N. C.; Dordick, J. S.; Linhardt, R. J.; Chao, J.; Wang, X. *Nat. Chem.* **2020**, *12*, 26−35.

(11) Chang, Y.; Wu, Z.; Sun, Q.; Zhuo, Y.; Chai, Y.; Yuan, R. *Anal. Chem.* **2019**, *91*, 8123−8128.

(12) Xu, Z.; Liao, L.; Chai, Y.; Wang, H.; Yuan, R. *Anal. Chem.* **2017**, *89*, 8282−8287.

(13) Li, C.; Li, H.; Ge, J.; Jie, G. *Chem. Commun.* **2019**, *55*, 3919−3922.

(14) Zhang, H.; Xu, X.; Jiang, W. *Chem. Sci.* **2020**, *11*, 7415−7423.

(15) Liang, C.-P.; Ma, P.-Q.; Liu, H.; Guo, X.; Yin, B.-C.; Ye, B.-C. *Angew. Chem., Int. Ed.* **2017**, *56*, 9077−9081.

(16) Peng, H.; Li, X.; Zhan, H.; Le, X. C. *Nat. Commun.* **2017**, *8*, 14378.

(17) Li, S.; Jiang, Q.; Liu, S.; Zhang, Y.; Tian, Y.; Song, C.; Wang, J.; Zou, Y.; Anderson, G. J.; Han, J.-Y.; Chang, Y.; Liu, Y.; Zhang, C.; Chen, L.; Zhou, G.; Nie, G.; Yan, H.; Ding, B.; Zhao, Y. *Nat. Biotechnol.* **2018**, *36*, 258.

(18) Zhu, C.; Liu, M.; Li, X.; Zhang, X.; Chen, J. *Chem. Commun.* **2018**, *54*, 10359−10362.

(19) Chai, H.; Miao, P. *Anal. Chem.* **2019**, *91*, 4953−4957.

(20) Wang, Z.-G.; Elbaz, J.; Willner, I. *Nano Lett.* **2011**, *11*, 304−309.

(21) Wu, N.; Wang, K.; Wang, Y.-T.; Chen, M.-L.; Chen, X.-W.; Yang, T.; Wang, J.-H. *Anal. Chem.* **2020**, *92*, 11111−11118.

(22) Xu, Z.; Chang, Y.; Chai, Y.; Wang, H.; Yuan, R. *Anal. Chem.* **2019**, *91*, 4883−4888.

(23) Jung, C.; Allen, P. B.; Ellington, A. D. *ACS Nano* **2017**, *11*, 8047−8054.

(24) Yang, L.; Dou, Y.; Sui, Z. X.; Cheng, H.; Liu, X.; Wang, Q. L.; Gao, P. F.; Qu, Y.; Xu, M. *Exp. Ther. Med.* **2020**, *19*, 603−610.
(25) Hirata, H.; Ueno, K.; Shahryari, V.; Tanaka, Y.; Tabatabai, Z. L.; Hinoda, Y.; Dahiya, R. *PLoS One* **2012**, *7*, No. e51056.
(26) Hemphill, J.; Govan, J.; Uprety, R.; Tsang, M.; Deiters, A. *J. Am. Chem. Soc.* **2014**, *136*, 7152−7158.
(27) Yang, L.; Tao, Y.; Yue, G.; Li, R.; Qiu, B.; Guo, L.; Lin, Z.; Yang, H.-H. *Anal. Chem.* **2016**, *88*, 5097−5103.
(28) Levicky, R.; Herne, T. M.; Tarlov, M. J.; Satija, S. K. *J. Am. Chem. Soc.* **1998**, *120*, 9787−9792.
(29) Zhang, J.; Zang, Q.; Yang, F.; Zhang, H.; Sun, J. Z.; Tang, B. Z. *J. Am. Chem. Soc.* **2021**, *143*, 3944−3950.
(30) Chen, M.; Luo, W.; Liu, Q.; Hao, N.; Zhu, Y.; Liu, M.; Wang, L.; Yang, H.; Chen, X. *Anal. Chem.* **2018**, *90*, 13647−13654.
(31) Wang, J.; Wang, D.-X.; Ma, J.-Y.; Wang, Y.-X.; Kong, D.-M. *Chem. Sci.* **2019**, *10*, 9758−9767.
(32) Peng, X.; Wen, Z.-B.; Yang, P.; Chai, Y.-Q.; Liang, W.-B.; Yuan, R. *Anal. Chem.* **2019**, *91*, 14920−14926.
(33) Zhou, H.; Zhang, J.; Li, B.; Liu, J.; Xu, J.-J.; Chen, H.-Y. *Anal. Chem.* **2021**, *93*, 6120−6127.
(34) Li, D.; Xu, Y.; Fan, L.; Shen, B.; Ding, X.; Yuan, R.; Li, X.; Chen, W. *Biosens. Bioelectron.* **2020**, *148*, 111826.
(35) Zhang, X.-l.; Yang, Z.-h.; Chang, Y.-y.; Liu, D.; Li, Y.-r.; Chai, Y.-q.; Zhuo, Y.; Yuan, R. *Chem. Sci.* **2020**, *11*, 148−153.
(36) Chen, S.-C.; Chen, K.-T.; Jou, A. F.-J. *Biosens. Bioelectron.* **2021**, *173*, 112815.

https://doi.org/10.1021/acs.analchem.1c02668
Anal. Chem. 2021, 93, 12981−12986